Crosslinker concentration effect on the poroviscoelastic relaxation of polyacrylamide hydrogels using depth-sensing indentation

C. Reinhards – Hervás, A. Rico, J. Rodríguez[*]

Durability and Mechanical Integrity of Structural Materials, Rey Juan Carlos University, Tulipán S/n, 28933, Móstoles, Madrid, Spain

ARTICLE INFO

ABSTRACT

The effect of crosslinker concentration on the mechanical behaviour of polyacrylamide based hydrogels is established by using depth sensing indentation. In this work, hydrogels are considered as poroviscoelastic solids, being viscoelasticity and poroelasticity taken into account at intermediate length scales such as those here explored. A constrained fitting method is derived to implement a multiplicative rule that accommodates the contribution of each deformation mechanism on the global material response. The proposed method is robust enough to properly separate poroelastic and viscoelastic contributions from relaxation curves measured at different indentation depths and strain rates. At the length scales here tested viscoelasticity appears as dominant, but the poroelastic contribution becomes increasingly important as the crosslinker concentration is reduced.

1. Introduction

Hydrogels are three – dimensional networks with a high ability to retain large amounts of water inside [1]. Swelling is a consequence of the thermodynamic affinity of the solvent by the hydrogel [2]. This hydrophilicity of the polymeric lattice is determined by the presence of hydrophilic groups such as –NH₂, –COOH, –OH, –CONH₂ y –SO₃H [3]. The polymer network adopts its stiffness by chemical and physical crosslinking methods [1]. Hydrogels accept water up to a thermodynamic equilibrium. Swollen hydrogels use to show a very high flexibility [3] with elastic moduli in the kPa range [4].

Among the main applications of hydrogels are drug delivery, tissue engineering, agriculture, and others [1–3,5]. In all of them, the mechanical properties largely determine their applicability [6,7]. Additionally, the behaviour of hydrogels has similarities with that of biological tissues [8–11] making their study and characterization rather interesting. In both cases, a combined response between viscoelasticity (VE) and poroelasticity (PE) is observed, giving rise to the so called poroviscoelastic (PVE) behaviour [8,12–16]. There are general models describing poroviscoelastic behaviour, which take into account both the viscoelastic and poroelastic effects in truly modelling framework [17, 18]. However, it is not clear how the chemical composition and the structural arrangement of the 3D lattice control the mechanical behaviour. More in depth, if the key microstructural features controlling the mechanical response of the hydrogels are revealed, tailoring of the properties could be accessible by modifying the chemistry and/or the structural parameters of the material.

The viscoelastic behaviour of hydrogels is given as a result of the conformational changes inside the polymeric structure in order to find an equilibrium state when it is subjected to a stress [12,13,19]. This response is controlled by a characteristic time which is independent on the test contact size [8,11,12,14,19–21], assuming that mesh size of the polymeric network is much smaller than the contact size used during a mechanical test [12,19].

The viscoelastic behaviour of hydrogels can be expressed as a standard viscoelastic solid model or Maxwell-Wierchert model [14,22–24]. In a relaxation test, load decreases continuously while displacement is set at a control value. In this conditions, the relaxation function, E(t), can be fitted to a Prony series following Eq. (1).

$$E(t) = E_\infty + \sum_{i=1}^{n} E_i \cdot \exp\left(\frac{-t \cdot E_i}{\eta_i}\right) \tag{1}$$

where E_∞ is the value after the viscoelastic process is relaxed, E_i and η_i the elastic modulus and the viscosity associated with each of the elements of the Maxwell - Wiechert model. Emphasize that $E_i/\eta_i = \tau_i$, where τ_i correspond to the viscoelastic relaxation time associated to each of the elements used.

Numerous studies [20,21,25] have described the viscoelastic behaviour of hydrogels by only using one single-term Prony series in Eq.

---

(1).

The poroelastic behaviour of hydrogels is due to the migration of the solvent through the pores of the polymeric mesh under mechanical stress [8,12,14,16,19,22,26,27]. This behaviour can be described by the theory of poroelasticity developed by M. Biot [26]. The migration rate of the solvent is determined by the intrinsic permeability of the solvent in the hydrogel, k, that is related to the diffusivity coefficient, D, by Eq. (2).

$$k = \frac{D \cdot (1 - 2\nu) \cdot \eta_s}{2(1 - \nu) \cdot G} \tag{2}$$

where ν is the Poisson ratio, G is the transverse elastic modulus of the hydrogel and η_s is the viscosity of the solvent contained in the hydrogel. (In the case of being water its value is $0.89 \cdot 10^{-3}$ Pa s) [28].

The poroelastic response is not only time - dependent [8,12,14,19, 27,28] but also size - dependent [8,19,27,28]. The fact that poroelasticity is size – dependent and viscoelasticity is not has governed the mechanical characterization of hydrogels in most of the work previously done. Contact size is usually changed in the mechanical tests to promote one response over the other [14,19].

One of the preferred method for characterizing hydrogels has been relaxation by uniaxial unconfined compression tests [25]. Mostly the experimental curve has been treated as poroelastic assuming that viscoelastic relaxation time is much smaller than the test duration. However, several problems have been observed because tests need to be too long and it is not so clear that viscoleasticiy can be completely neglected.

Yuhang Hu et al. [19] and Edwin E. Chan et al. [16] used macroscale indentation to characterize hydrogels through the predominance of the poroelastic response. It was determined that the poroelastic load relaxation function $g(\phi)$, is not only dependent on the indentation size, a^2, but also on the indenter geometry. Using numerical simulation explicit poroelastic relaxation equations for spherical indentation tests were provided (Eqs (3) and (4)).

$$\frac{P_{PE}(t) - P(\infty)}{P_{PE}(0) - P(\infty)} = g(\phi) \tag{3}$$

Where $\phi = D \cdot t / a^2$ and

$$g(\phi) = 0.491 \exp\left(-0.908\sqrt{\phi}\right) + 0.509 \exp(-1.679\phi) \tag{4}$$

Micro/nanoscale load relaxation indentation tests have been also performed with hydrogels [21,23] by considering the material as a viscoelastic solid. Matteo Galli et al. [21] perform nanoscale and microscale indentation tests treating the experimental response as viscoelastic and obtaining by finite element simulation the poroelastic properties. Jessica D. Kaufman et al. [24], Wei Hu et al. [27] and Z. Ilke Kalcioglu et al. [28] did an experimental comparison between the mechanical behaviour of hydrogels at macro- and microscale.

Commonly, the mechanical characterization of hydrogels has been oriented to a simplification of the actual behaviour. A significant advance in the study of the poroviscoelastic response would be the development of a methodology capable of separating and quantifying the viscoelastic and poroelastic contributions without the need to neglect any of them.

Edwin P. Chan et al. in Ref. [16] propose an additive poroviscoelastic interaction following Eq. (5).

$$P_{PVE}(t) = P_{VE}(t) + P_{PE}(t) \tag{5}$$

On the other hand, Daniel G. T. Strange et al. [12] propose a multiplicative poroviscoelastic interaction according to Eq. (6).

$$P_{PVE}(t) = \frac{P_{VE}(t) \cdot P_{PE}(t)}{P_\infty} \tag{6}$$

Although it is not clear the validity of Eqs (5) and (6), it seems that the additive rule can be used when characteristic times for poroelastic and viscoelastic responses are largely different for the particular length scale. However, if the characteristic times of each phenomenon are overlapped, the multiplicative rule appears as the best option describing how the deformation mechanisms interact on each other.

It is important to note that all of the previous expressions are based on continuum mechanics and it is hardly to know how the material features affect the parameters governing constitutive equation of hydrogels. Several efforts have been made to enlighten the influence of microstructural parameters on mechanical behaviour; but, to the authors knowledge, most of them does not study the poroviscoelastic behaviour of the materials.

In this work, we study polyacrylamide based hydrogels at the micro length scale by means of depth sensing indentation. It is assumed that both deformation mechanism, poroelasticity and viscoelasticity, are activated during the test. Crosslinking of the hydrogels should be one of the most relevant phenomena affecting the mechanical behaviour of these materials. Consequently, the main objective of this work is to determine the influence of crosslinker concentration on the poroviscoelastic performance of the polyacrylamide hydrogels.

2. Experimental methodology

2.1. Materials

2.1.1. PAAm hydrogels

Cross - linked polyacrylamide hydrogels were synthesized using solution polymerization. Two types of polyacrylamide hydrogels of different composition were synthesized, 15% T - 6% C and 15% T - 0.6% C, following relations Ec. 7 and Ec. 8 collected by Chirani N. et al. (2016) [2] and Aleksandra K. Denisin et al. (2016) [4].

$$\%T\,(w\,/\,v) = \frac{weight\ of\ monomer(g) + weight\ of\ x - crosslinker\ (g)}{total\ volume\ (mL)} \tag{7}$$

$$\%C\,(w\,/\,w) = \frac{weight\ of\ x - crosslinker\ (g)}{weight\ of\ monomer\ (g) + weight\ of\ x - crosslinker(g)} \tag{8}$$

The weight proportions for each composition of acrylamide monomer (Merck Group, ref. 8.00830) and *N,N'*-Methylenebisacrylamide cross – linker (Merck Group, ref. 1.01546) were put into mili – Q water in a beaker glass until their complete dissolution. The dissolution was helped by a magnetic stirrer. Once the *N,N'*-Methylenebisacrylamide clusters was dissolved, N,N,N′,N′-Tetramethylethylendiamine polimerization accelerator (Merck Group, ref. 1.10732) and Amonium Persulfate reaction initiator (Hach, ref. 11201H) were added to the solution in a weight proportion of 0.0046 and 0.0045 times the weight of acrylamide, respectively. The precursor solution was poured into PMMA moulds covered by glass bases enclosing it in a cylindrical cavity (R = 5 mm, h = 6 mm) where the hydrogel polimerization was carried out. After 24 h the polymerized hydrogels samples were demoulded and hydrated in milli – Q water for another 24 h before being tested.

2.1.2. PAAm xerogels synthesis

Two types of xerogels have been synthesized corresponding to the PAAm hydrogels of composition 15% T - 6% C and 15% T - 0.6% C. The synthesis method of these hydrogels exposed in the previous section has been followed, but instead of pouring the precursor solution into moulds, it has been introduced into 1 cm diameter syringes where they have cured. Once cured, they have been cut into cylindrical test tubes and left to dry at room temperature for a minimum time of 2 weeks. In the drying process, a permeable mesh has been used to impose equal boundary conditions on all of the free surfaces, avoiding evaporation gradients and, therefore, residual stresses that deform or stresses the specimen.

2.2. Depth sensing indentation

Load – relaxation microindentation tests were carried out using an Agilent G200 indenter with a Keysight XP indenter head with a 500 mN load cell. Experiments run two segments under displacement control. During first one, displacement of the indenter was linearly increased on the sample at a prescribed strain rate up to reach the maximum depth programmed in the test. Afterwards, during the second segment, displacement was held during 1200 s at a constant value equal to that reached in the previous part. Load was recorded during the whole duration of the experiment revealing the relaxation behaviour of samples during the second branch of the test. All tests were performed with a temperature control of 20 °C. A ruby spherical indenter (800 μm of radius) has been used.

In order to establish the influence of the contact size and the strain rate on the poroviscoelastic behaviour under relaxation of hydrogels, three penetration depths and three strain rates during the loading ramp were programmed for these materials. Note that contact size can be estimated for spherical indentation as the square root of the product between the indenter radius and the penetration depth. All tests in hydrogels were conducted in a liquid cell under immersion in milli– Q water to maintain the saturation condition in the samples during the whole test. In contrast, xerogels were tested at dry condition. Three maximum penetration depths and two strain rates were used for xerogels.

To ensure statistical validation of the experimental campaign, tests were repeated at each experimental condition. Table 1 collect experimental details used in this work.

3. Results

Fig. 1 shows the loading segment and the relaxation curves measured for polyacrylamide hydrogels at three maximum penetration depths and at three prescribed strain rates during the loading ramp for each material. Although a certain degree of dispersion is observed among different samples, it is considered that a good control is achieved and properly maintained during the test. For all tests, a good repeatability is observed, allowing the calculation of an average curve for each experimental condition (black curves in Fig. 1). The average curves at each penetration depth will be used throughout the rest of the manuscript.

As expected, once the maximum depth is reached and displacement is held to observe the samples relaxation, load decreases with time and contact size, showing the typical load relaxation curve for these materials. It is evident that crosslinker concentration clearly affects to the stiffness of the material. The higher the concentration, the higher the measured loads for the same indentation depth. Strain rate of the loading ramp also have an influence on the relaxation curves. For both hydrogels, the maximum load reached at the end of the loading ramp is higher as the strain rate of the loading ramp is increased. On the other hand, the equilibrium is found during the relaxation by reaching a constant load value well before 1200 s. Although samples are not relaxing exactly at the same time, all of them relaxes at a similar range from 100 to 300 s. Relaxation times are slightly affected by the strain rate of the loading segment. It seems that tests performed at higher strain rate relaxed at lower times than those measured at lower strain rates. However, it is difficult to assess the exact time relaxation scale by direct observation of the curves, thus, a more in depth analysis is needed. In other words, experimental curves by themselves do not allow for a clear discrimination between deformation mechanisms or for a ranking between materials focused on the contributions of the poroelastic or viscoelastic phenomena.

Fig. 2 includes relaxation curves for the xerogels 15%T - 6%C and 15%T – 0.6%C polyacrylamide samples measured at three penetration depths and two strain rates imposed during the loading segment. Displacement control is also well achieved, and also the repeatability is acceptable allowing the calculation of average curves for each experimental condition (black curves in Fig. 2).

As expected, measured loads are increased by one order of

Table 1
Experimental details for depth – sensing indentation tests.

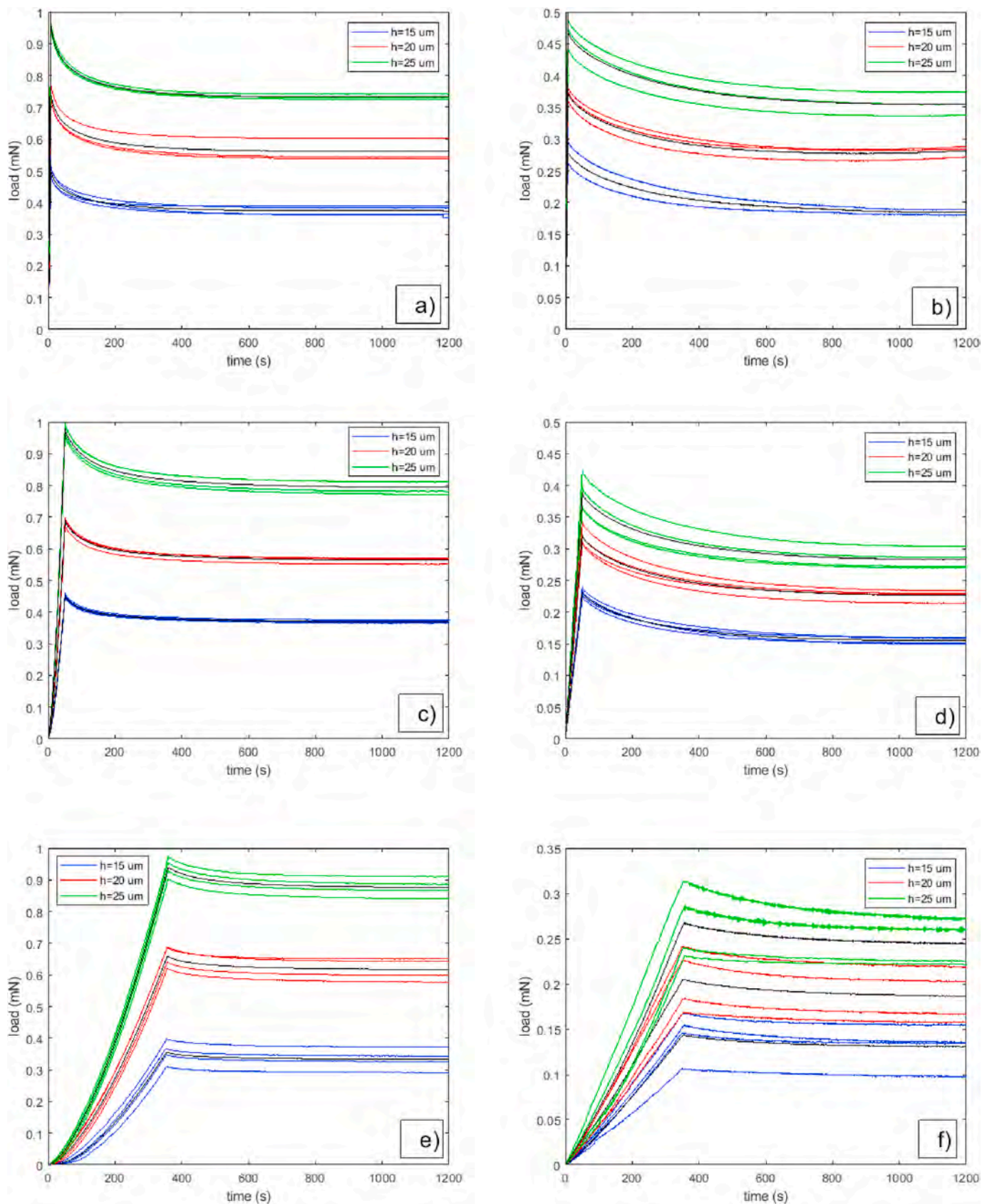| Material	Condition	Loading time	Strain rate during the loading ramp	Maximum penetration depth (h_{max})	Contact size during relaxation $(R \cdot h_{max})^{0.5}$	Holding Time during relaxation	No. Tests
(−)	(−)	(s)	(s^{-1})	(μm)	(μm)	(s)	(−)
15%T-6%C	Hydrogel	6	0.17	25	141	≈1200	3
				20	126		3
				15	110		4
		50	0.02	25	141		4
				20	126		4
				15	110		4
		360	0.0027	25	141		4
				20	126		4
				15	110		4
	Xerogel	50	0.02	1	28		4
				0.75	24		4
				0.5	20		2
		360	0.0027	1	28		4
				0.75	24		4
				0.5	20		4
15%T-0.6%C	Hydrogel	6	0.17	25	141		3
				20	126		3
				15	110		2
		50	0.02	25	141		4
				20	126		4
				15	110		4
		360	0.0027	25	141		4
				20	126		4
				15	110		4
	Xerogel	50	0.02	1	28		4
				0.75	24		4
				0.5	20		3
		360	0.0027	1	28		4
				0.75	24		4
				0.5	20		4

Fig. 1. Experimental load – vs time curves a) 15%T – 6%C polyacrylamide hydrogel measured at 0.17 s^{-1} of strain rate during the loading ramp. B) 15%T – 0.6%C polyacrylamide hydrogel measured at 0.17 s^{-1} of strain rate during the loading ramp c) 15%T – 6%C polyacrylamide hydrogel measured at 0.02 s^{-1} of strain rate during the loading ramp. D) 15%T – 0.6%C polyacrylamide hydrogel measured at 0.02 s^{-1} of strain rate during the loading ramp. E) 15%T – 6%C polyacrylamide hydrogel measured at 0.0027 s^{-1} of strain rate during the loading ramp. F) 15%T – 0.6%C polyacrylamide hydrogel measured at 0.0027 s^{-1} of strain rate during the loading ramp.
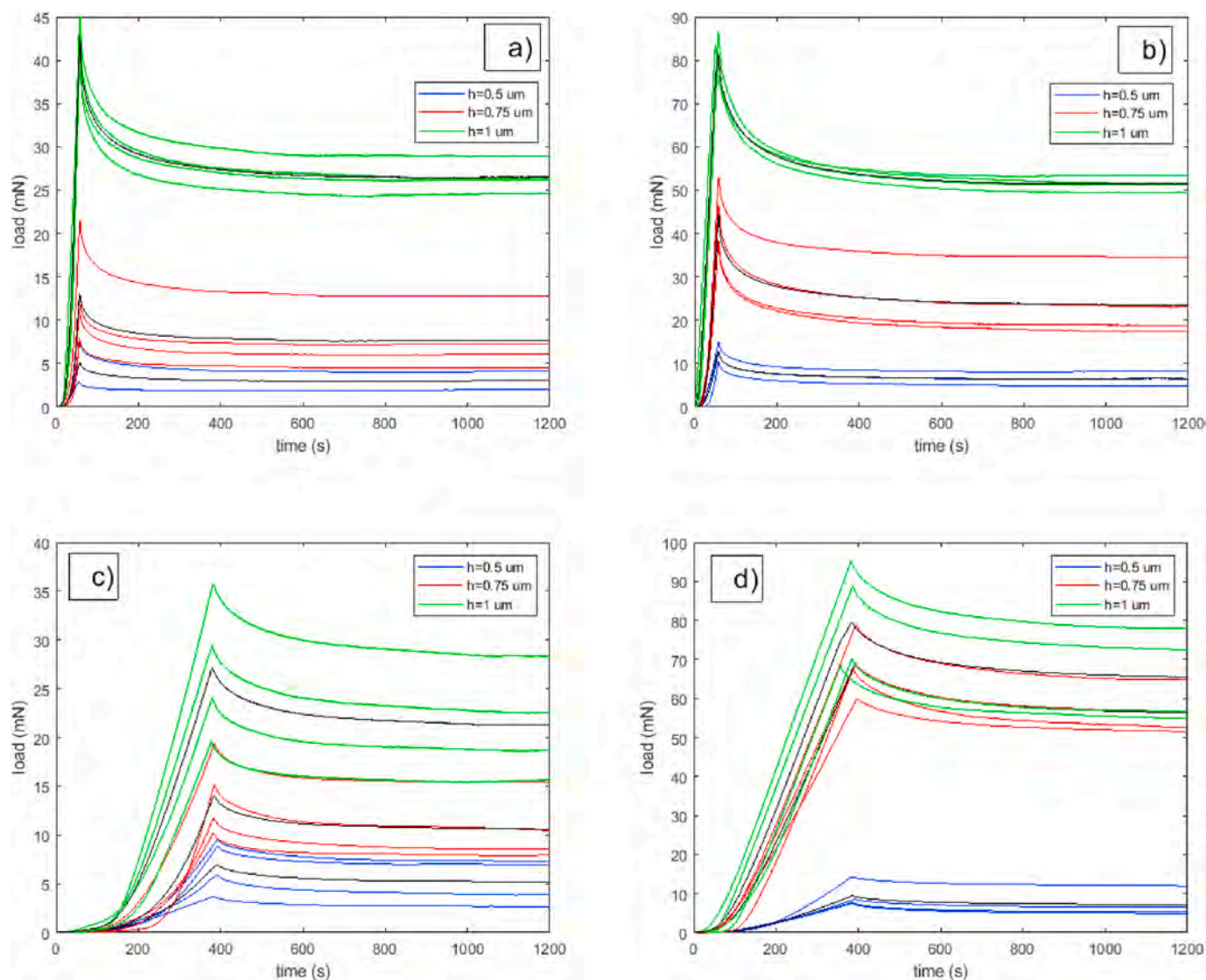
Fig. 2. Experimental Load vs time curves. A) 15%T – 6%C polyacrylamide Xerogel measured at 0.02 s^{-1} of strain rate during the loading ramp. B) 15 %T – 0.6%C polyacrylamide Xerogel measured at 0.02 s^{-1} of strain rate during the loading ramp. C) 15%T – 6%C polyacrylamide Xerogel measured at 0.0027 s^{-1} of strain rate during the loading ramp. D) 15%T – 0.6%C polyacrylamide Xerogel measured at 0.0027 s^{-1} of strain rate during the loading ramp.

magnitude compared to those of hydrogels in Fig. 1 mesaured at same strain rate, revealing that xerogels are much stiffer than hydrogels counterparts. Additionally, strain rate of the loading ramp affects in the same way than that pointed out for hydrogels. The higher the strain rate, the higher the maximum load measured prior the relaxation segment. Again, it is difficult to stablish a correlation between strain rate and relaxation time, but it seems that curves performed at lower strain rate of the loading ramp are shifted to higher relaxation times. However, a more detailed analysis of the experimental curves is required.

4. Discussion

4.1. On the relative importance of the viscoelastic and poroelastic contributions in polyacrylamide hydrogels

Load curves presented in Figs. 1 and 2 have to be explained attending to the relaxation phenomena that are activated in the materials during the indentation test. As was stated before, hydrogels are considered time – dependent materials due to the concurrence of two types of relaxation mechanisms: on one side, the spacial lattice is formed by a polymer presenting an intrinsic viscoelastic behaviour; on the other hand, water

retained inside the 3D polymeric network is forced to migrate during the load application, driving to the poroelastic contribution. Competition between both are stablished in terms of a length scale, because poroelastic behaviour is size - dependent, while viscoelastic is not.

Using the concept of normalization a master curve is built computing a dimensionless load as was stated in previous works.

$$P_{norm} = \frac{P(t) - P_\infty}{P_0 - P_\infty} \tag{9}$$

where P_∞ is the asymptotic load value when the sample is fully relaxed and P_0 is the instantaneous load measured at the initial step of the relaxation.

This methodology is based on the fact that the viscoelastic contribution is not size - dependent, and once the load is normalized, the curves of viscoelastic materials measured at different penetration depths should collapse in a single one. However, normalization for a poroelastic material would also require dividing the time by the contact size at different penetration depths. In a poroviscoelastic material, the load normalization following Eq. (9) can be used as a first insight in the relative importance of both deformation mechanisms at the particular length scale used in the test. All curves tend to collapse in a single trend

if viscoelasticity is the dominant mechanism. However, as the poroelastic contribution becomes more important, an appropriate normalization requires to use the contact size.

Fig. 3 comprises the normalization plots for the hydrogels and xerogels tested in this work. Fig. 3a and b shows the load normalization plots for the polyacrylamide based hydrogels. For both materials, when tests obtained at the same strain rate for the loading ramp are observed, a quasi – single master curve is displayed by the fully collapse of single curves measured at different penetration depths. Thus, hydrogels seem to show a noticeable viscoelastic behaviour at this length scale. In addition, it is interesting to note that normalized plots are slightly shifted to higher relaxation times as the strain rate is decreased. On the other side, Fig. 3c and d presents normalized plots for xerogels. As these materials are tested in dry conditions, viscoelastic behaviour should be the key mechanism explaining the relaxation behaviour for this materials. As expected, despite of the strain rate value used to perform the tests, single experiments measured at different contact sizes, but at the same strain rate, form a single master curve when they are normalized; confirming the previous hypothesis. However, there are some different behaviours among materials. While highly crosslinked hydrogel 15% T - 6%C (Fig. 3a) shows a unique trend at each strain rate for all penetration depths, very similar to that observed for xerogels (Fig. 3c and d), low crosslinked hydrogels curves are not perfectly collapsed (Fig. 3b).

Furthermore, relaxation time is clearly displaced to higher values for the low crosslinked hydrogels.

In more detail, Fig. 4 shows a comparison of normalized plots between hydrogels and xerogels tested at the same strain rate. Two main observations arises from these plots. Firstly, xerogels behaves in a very similar way when normalized loads are used. They are placed at the same path independently on the crosslinker concentration or on the strain rate. Secondly, hydrogels present a clear difference when normalized loads are compared to those of xerogels. Highly crosslinked hydrogel follow a very similar normalized trend than those exhibited by xerogels. However, low crosslinked hydrogel curves are clearly shifted to higher relaxation times far from those showed for the other materials. These observations are systematic despite of the strain rate used during the tests.

As was stated before, as the xerogels samples are tested in dry conditions, viscoleasticity should be responsible for the entire relaxation curve measured in these cases. Thus, it can be concluded that the viscoelastic charatderistic relaxation time is directly related to the polymer nature of the 3D network, and not to the crosslinker concentration. Secondly, once the load is normalized, highly crosslinked hydrogel is nearly placed at the same curve than those displayed by the xerogels, pointing out that this material presents a mainly viscoelastic behaviour at the length scale here tested. Elseways, the low crosslinked hydrogel is
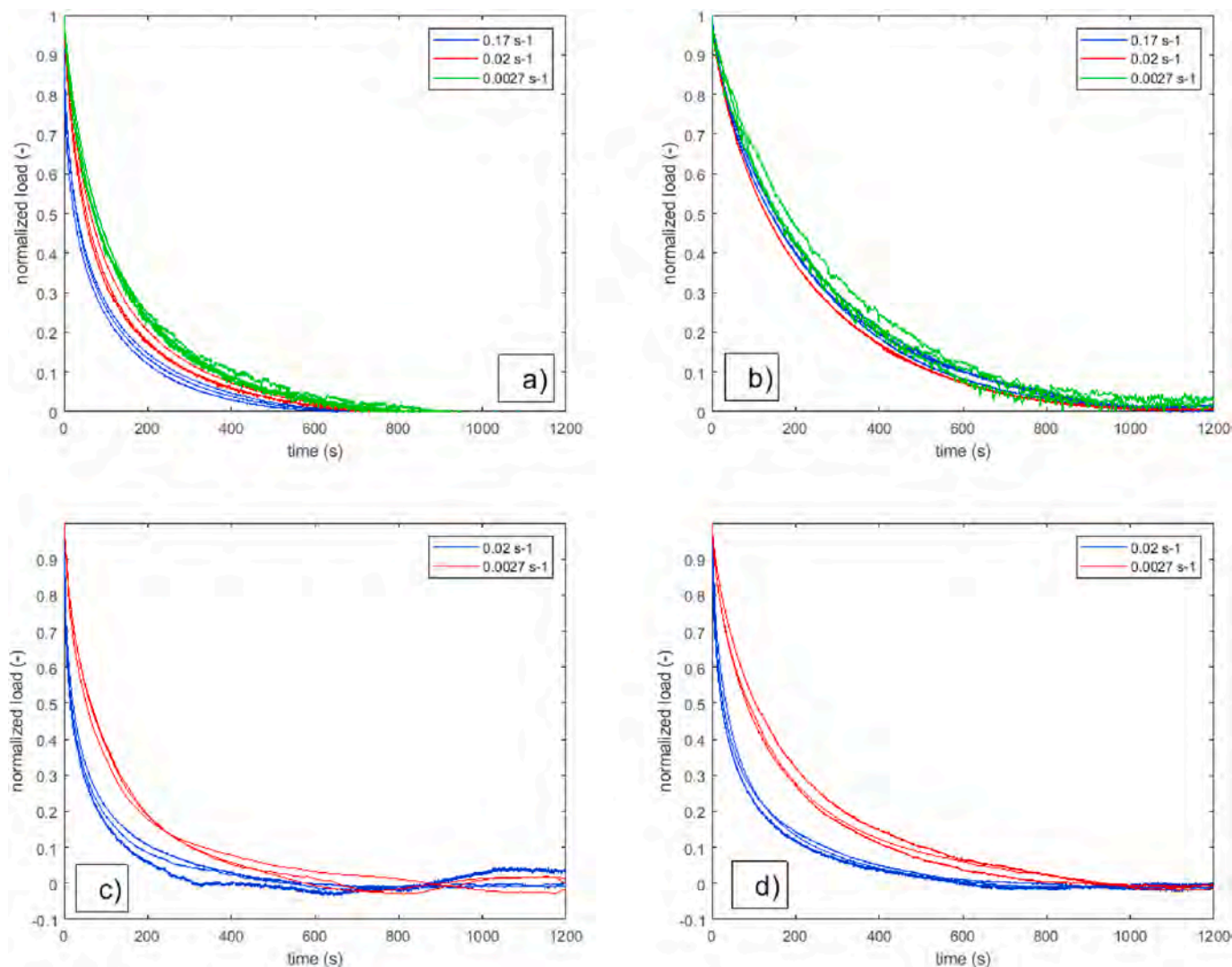

Fig. 3. Load normalization plots of the relaxation segment for the materials studied. A) 15 %T – 6%C hydrogel. B) 15 %T – 0.6%C hydrogel. C) 15 %T – 6%C xerogel. D) 15 %T – 0.6%C xerogel.
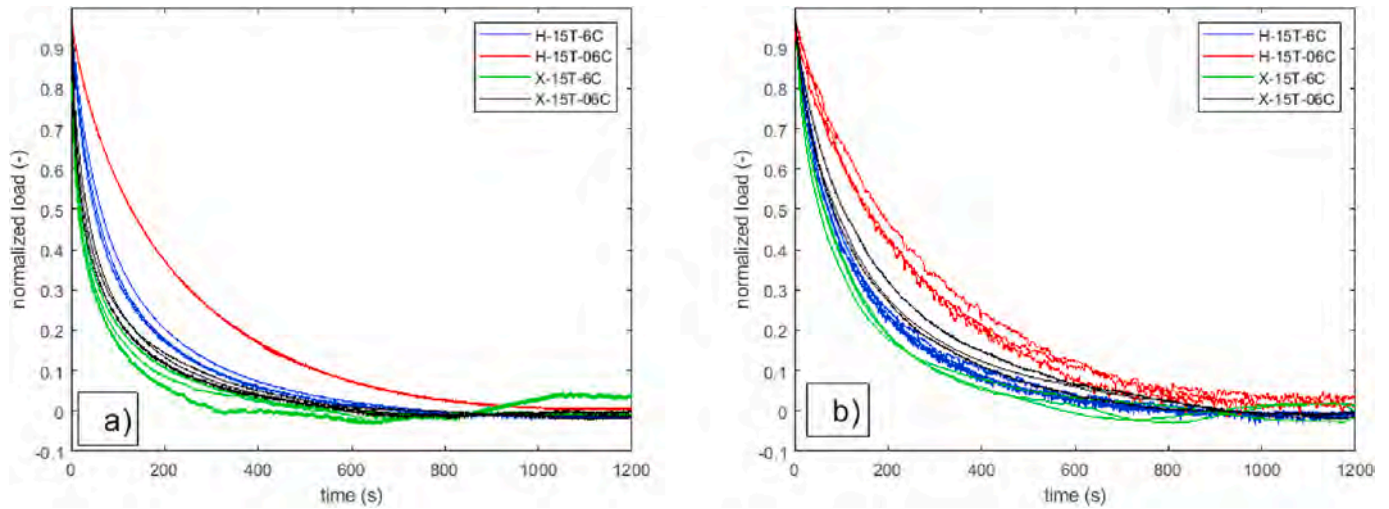
Fig. 4. Comparison between load normalization plots for hydrogels and xerogels a) strain rate of 0.02 s–1. B) strain rate of 0.0027 s–1.

clearly shifted to higher relaxation times. Thus, its behaviour should be explained attending to the poroelastic contribution. In other words, for low crosslinked hydrogels, viscoelasticity does not seem to be the unique deformation mechanism that is activated during the mechanical relaxation.

At this stage, we can affirm that by reducing the crosslinker concentration, an increment of the relative contribution of the poroelastic deformation mechanism is achieved. However, this is a qualitative conclusion obtained from direct observation of the experimental curves and the normalization plots. A deeper analysis is needed to quantify the ratio between poroelasticty and viscoelasticity on the global mechanical behaviour.

4.2. Fitting constrained method

From the experiments showed in the previous section one must conclude that the poroelastic and viscoleastic contributions in poly-acrylamide hydrogels are overlapped for the contact size tested because a single relaxation is observed. According to Ref. [16], if relaxations corresponding to different deformation mechanisms are not overlapped because characteristic relaxation times are enough different, material transits for two different realxation phenomena that can be directly observed in the experimental curve. It is clear that this is not observed in the experimental trends measured for polyacrylamide hydrogles at this length scale. Accepting this, two main questions remain. Is competition between poroelasticity and viscoelasticity dependent on the composition of hydrogels? Can the poroelastic and viscoelastic contributions be discriminated? Actually, both questions could be answered developing a method to properly discriminate both deformation mechanisms from the experimental curve. Once the contributions are known, the influence of the hydrogels concentration can be determined.

The multiplicative rule in Eq. (6) can be used when poroelastic and viscoelastic relaxations are overlapped during the relaxation segment. In the case of poroelasticity, Eqs. (3 and 4) express the time and size dependence of the load. This can be also particularized for a spherical indentation. Viscoelastic contribution can be modelled using the well known Prony series. In this case a two – term were used trying to characterize the short and medium/long time scales. If theses constitutive relations are included in Eq. (6), a fitting model can be derived (Eq. (10)). A detailed deduction of this model is included in Appendix 1.

$$
\begin{aligned}
P_{PVE}(t) - P_\infty &= \left(P_0^{VE} - P_\infty\right)\left[Aexp\left(-t/\tau_{VE1}\right) + (1-A)exp\left(-t/\tau_{VE2}\right)\right] \\
&+ P_\infty(1 - 2\nu_\infty)\left[0.491\exp\left(-0.908\sqrt{Dt/Rh}\right)\right. \\
&+ \left.0.509\exp\left(-1.679\,Dt/Rh\right)\right] + \left(P_0^{VE}\right. \\
&- P_\infty\left)\left[A\,exp\left(-t/\tau_{VE1}\right)(1-A)\,exp\left(-t/\tau_{VE2}\right)\right] \cdot (1\right. \\
&- 2\nu_\infty\left)\left[0.491\exp\left(-0.908\sqrt{Dt/Rh}\right) + 0.509\exp\left(\right.\right.\right. \\
&- \left.\left.1.679\,Dt/Rh\right)\right]
\end{aligned}
$$

$$(10)$$

It must be said that this is a highly parametrized model in which six coefficients have to be fitted: viscoelastic pre-exponential factor, A, instantaneous load of the viscoelastic contribution, P_0^{VE}, characteristic viscoelastic relaxation times, τ_{VE1} and τ_{VE2}, diffusivity, D, and Poisson ratio when the material is fully relaxed, ν_∞. First four coefficients are related to the viscoelastic contribution and the last two parameters are linked to the poroelastic one. Obviously, a free fit of Eq. (10) to the experimental data is not recommended because it is difficult to evaluate how good the fit is. Actually, a measure of the robustness of a fitting method can be checked by using experimental data from a material in which the mechanical response is known. As was stated before, xerogels have to be considered purely viscoelastic materials because they are mechanically tested at dry conditions. However, if a free fit of Eq. (10) is applied to the experimental data from xerogels a non – sense solution is obtained as it is shown in Fig. 5.

As the model includes a poroelastic segment, fit is forced to obtain Diffusivity and Poisson ratio. As a result, best fit provides a minor, but still significant, poroelastic contribution in xerogels for all experimental conditions. Even when it is known that the material should be exclusively viscoelastic because any fluid is present. Surprisingly, square of the correlation factor is computed above of 0.997 for these fits. A robust fitting method should deliver a model solution with no poroelastic contribution when it is used to explain curves measured in xerogels.

To circumvent this problem, a mathematical restriction that constraints the fitting model is proposed. This constraint can be derived precisely from the same multiplicative rule in Eq. (6) and relies again on the fact that poroelasticity is size - dependent and viscoelasticity is not. The load normalization method needed for each mechanisms allows
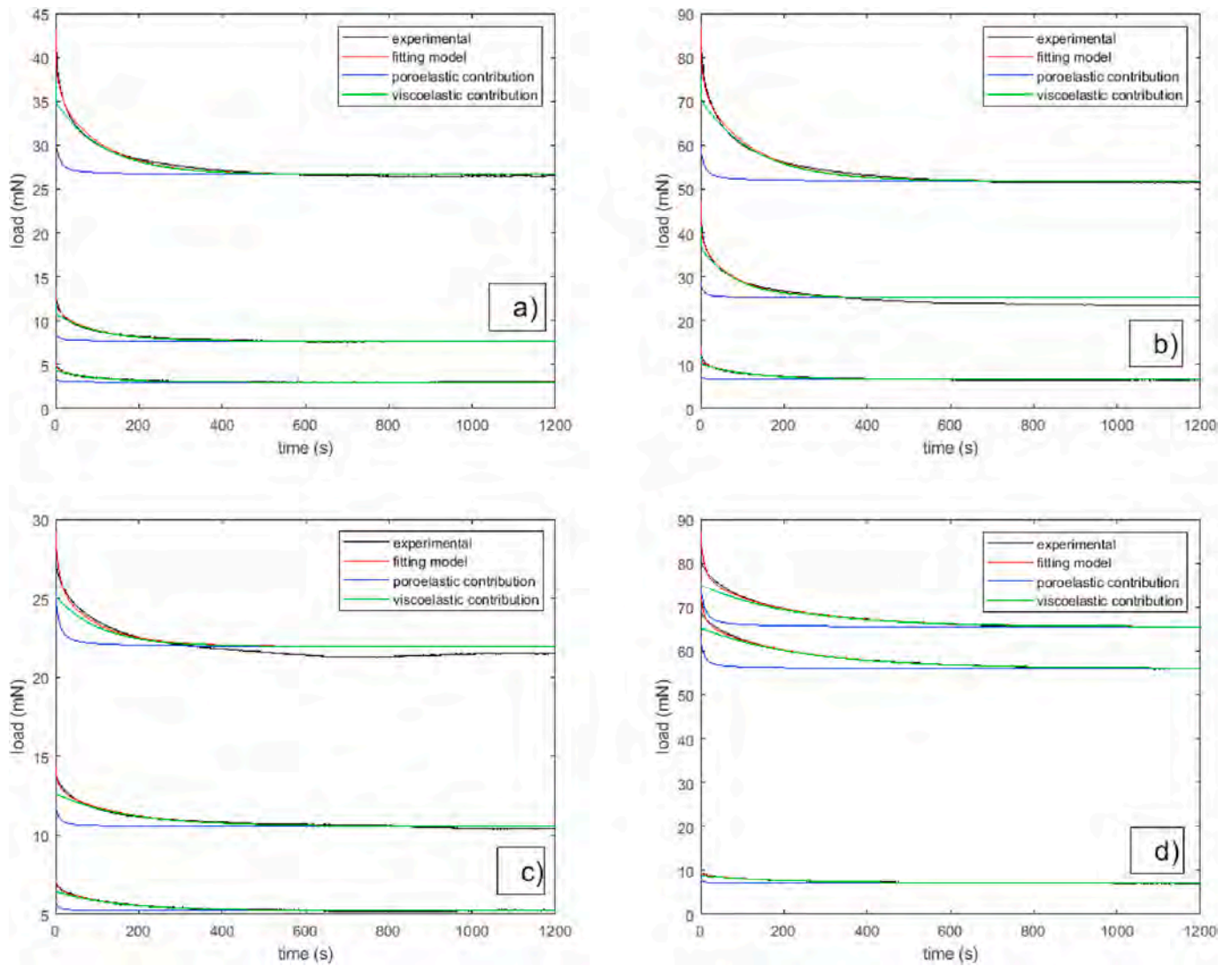
Fig. 5. Best free fit of model in Eq. (10) applied to average relaxation curves of Xerogels. Curves from up to down in each plot corresponds to penetration depths maintained at 1 μm, 0.75 μm and 0.5 μm, respectively. A) 15% T – 6% C xerogel tested at 0.02 s^{-1} b) 15% T – 0.6% C xerogel tested at 0.02 s^{-1}. C) 15% T – 6% C xerogel tested at 0.0027 s^{-1}. D) 15% T – 0.6% C xerogel tested at 0.02 s^{-1}.

discriminating them. If the multiplicative rule is subsequently normalized by viscoelastic and poroelastic contributions, a very interesting relation between tests performed at different contact sizes can be derived (Eq. (11)). A detailed deduction is collected in Appendix 2.

$$\frac{P_{PVE}(t)_{hi}}{P_{PVE}(t)_{hj}} - \frac{P_{\infty hi}}{P_{\infty hj}} + \frac{P_{VE}(t)_{hi}}{P_{VE}(t)_{hj}} - \frac{P_{PE}(t)_{hi}}{P_{PE}(t)_{hj}} = 0 \qquad (11)$$

Where $P_{PVE}(t)$ is the experimental load measured for a poroviscoelastic material, P_{∞}, is the load when the material is fully relaxed, $P_{VE}(t)$ is the load contribution for the viscoelastic mechanism, $P_{PE}(t)$ is the load contribution for the poroelastic mechanism, and *hi, hj* states for tests performed at two different contact size or penetration depths or even two indentations using different indenter geometries. At least two different relaxation tests at different penetrations must be carried out to apply the constraint. Interestingly, Eq. (11) can be derived independently on the particular constitutive equation used for the viscoelastic or the poroelastic contribution. Advantageously, the first two terms in Eq. (11) are experimentally measured, while the last two terms are obtained once the model in Eq. (10) is fitted to experimental data. This is precisely why Eq. (11) constraints the fit. The problem now is to determine six fitting coefficients to provide the poroelastic and the viscoelastic contributions that minimize the difference between experimental

measurements and fitted responses in Eq. (11), when different penetration depths are tested.

A depth sensing indentation experiment at three different contact sizes was performed, and using Eq. (11) three constraint conditions can be calculated for this particular work by combining results of different penetration depths, as it is presented in Eq. (12).

$$f_{12}(t) = \frac{P_{PVE}(t)_1}{P_{PVE}(t)_2} - \frac{P_{\infty 1}}{P_{\infty 2}} + \frac{P_{VE}(t)_1}{P_{VE}(t)_2} - \frac{P_{PE}(t)_1}{P_{PE}(t)_2} = 0$$

$$f_{13}(t) = \frac{P_{PVE}(t)_1}{P_{PVE}(t)_3} - \frac{P_{\infty 1}}{P_{\infty 3}} + \frac{P_{VE}(t)_1}{P_{VE}(t)_3} - \frac{P_{PE}(t)_1}{P_{PE}(t)_3} = 0 \qquad (12)$$

$$f_{23}(t) = \frac{P_{PVE}(t)_2}{P_{PVE}(t)_3} - \frac{P_{\infty 2}}{P_{\infty 3}} + \frac{P_{VE}(t)_2}{P_{VE}(t)_3} - \frac{P_{PE}(t)_2}{P_{PE}(t)_3} = 0$$

where 1, 2 and 3 states for the three different penetration depths and $f_{ij}(t)$ is a contraction to express the constraint factor for the combination of penetrations *i* and *j*. According to Eqs. (11) and (12), the constraint factor should be null at each testing time despite of the particular couple of penetration depths used. Thus, a general fitting condition for the fit can be derived combining tests performed at an arbitrary number of contact sizes by adding the individual constraints:

$$\sum_{\substack{i=1 \\ j=1}}^{n} f_{ij}(t) = 0; i \neq j \tag{13}$$

In this work, Eq. (13) is particularized as:

$$f_{12}(t) + f_{13}(t) + f_{23}(t) = 0 \tag{14}$$

Constraint in Eq. (14) must be included in the fitting process. However, this means that fitting algorithm has to be changed. In this work, a procedure based on a sensitivity analysis of one of the fitting coefficients, the short viscoelastic relaxation time, was implemented. As a two – term Prony series was used to model the viscoelastic behaviour, one of the relaxation times accounts for the conformational changes occurred in the polymeric chains at very short times. In particular, literature points out that for polyacrylamide hydrogels the short viscoelastic time should be in the order of 1 s or lower. Consequently, prior to the fitting calculation the value of short viscoelastic time was fixed between 0.01 and 10 s. Afterwards, the fit at the three penetration depths experimentally measured was performed to obtain the other five fitting coefficients by the least squares methodology, selecting those with the best correlation number R^2. Once the fit is obtained for each short

viscoelastic time value, the poroelastic and the viscoelastic contribution can be derived for each penetration depth. Finally, Eq. (14) can be used to compute the global constraint factor in each fit. One thousand values for the short viscoelastic time were swept in the range used. Therefore, one thousand global constraint factors were estimated following Eq. (12)–14. The final step is to select the fitting model corresponding to the lowest value of the global constraint factor.

Fig. 6, in contrast to Fig. 5, shows results obtained when the global constraint factor is used in the fitting calculations for polyacrylamide xerogels using previous procedure. It is clear that the constraint factor allows to obtain a well based result for all experimental conditions. In this case, despite of the penetration depth or the strain rate, xerogels are interpreted as purely viscoelastic materials. Green (viscoelastic contribution) and red (fitting model) curves in Fig. 6 completely overlap, pointing out that fitting is only dependent on viscoelastic properties. Additionally, as the model is forced to compute a poroelastic contribution, the constrained fitting method drives to a non-time dependent curve (blue line in Fig. 6) reaching from the very beginning the P_∞ value. In other words, constrained fitting is able to properly discriminate the viscoelastic and poroelastic contributions from the experimental curves. The global constraint factor obtained for each fit using Eq. (14) is maintained at a low value for the whole time range. Finally, fitting
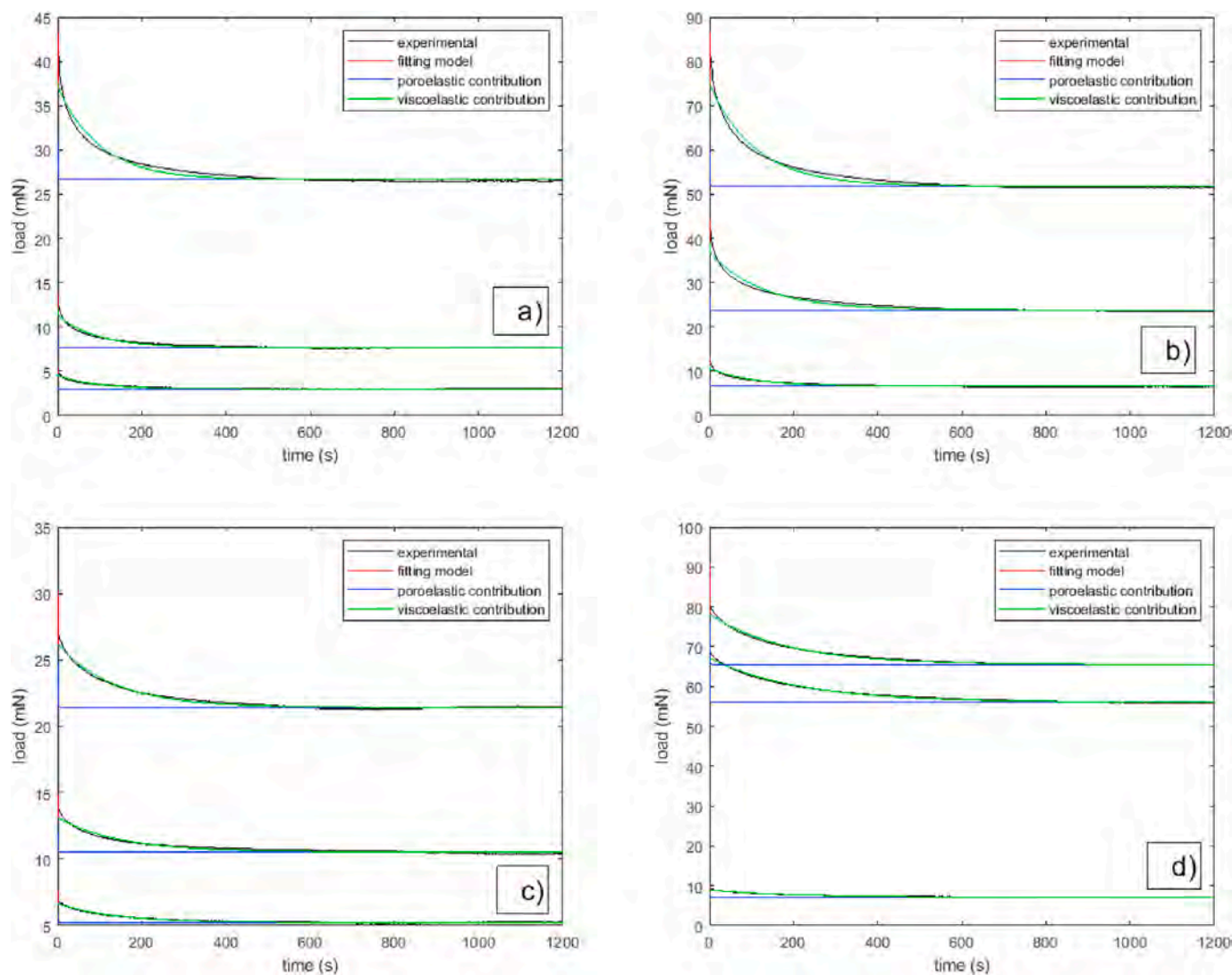

Fig. 6. Constrained fit of model in Eq. (10) applied to average relaxation curves of Xerogels. Curves from up to down in each plot corresponds to penetration depths maintained at 1 µm, 0.75 µm and 0.5 µm, respectively. A) 15% T – 6% C xerogel tested at 0.02 s^{-1} b) 15% T – 0.6% C xerogel tested at 0.02 s^{-1}. C) 15% T – 6% C xerogel tested at 0.0027 s^{-1}. D) 15% T – 0.6% C xerogel tested at 0.0027 s^{-1}.

coefficients for xerogels at each condition are included in Table 1. Note that short and long term viscoelastic relaxation times and pre-exponential factor, A, are very similar between xerogels despite of the crosslinker concentration; which is in agreement with plots showed at Fig. 4, justifying why normalized curves measured at the same strain rate from xerogels are shifted to the same master curve when load is normalized.

4.3. Discriminating viscoelastic and poroelastic contributions in hydrogels

The fitting procedure in the previous section was applied to poly-acrylamide based hydrogels. Fig. 7 shows the experimental curve, the fitting model and the viscoelastic and poroelastic contributions for each material, penetration depth and strain rate. Fig. 7a, c and 7e present results for 15% T – 6% C hydrogels at different strain rates. It can be seen that, despite of the strain rate of the loading ramp, viscoelastic contribution explains the majority of the experimental curves for this material. However, there is still a poroelastic part which presents a minor importance at the initial stages of the relaxation curve. Additionally, poroelastic contribution is fully relaxed at very short times, pointing out that highly crosslinked hydrogel can be understood as a quasi – visco-elastic solid.

Table 2 includes fitting coefficients for this material. Short and long viscoelastic relaxation times and pre-exponential factor of the Prony series are very similar to those computed for xerogels at the same experimental conditions, explaining why 15% T – 6% C hydrogel collapsed to the same normalized curve as xerogels in Fig. 4. On the other side, in Fig. 7b, d and 7f viscoelastic and poroelastic contributions for low crosslinked hydrogel are included for all experimental conditions. Although viscoelasticity remains as the most relevant deformation mechanism for these materials at all experimental conditions; interestingly, poroelastic contribution is much more important than that observed for highly crosslinked hydrogel. For some penetration depths and strain rates, blue lines in Fig. 7 (poroelastic parts) overcome green lines (viscoelastic parts) at the shorter times, pointing out that the first relaxation stages in low crosslinked hydrogels should be attributed to the poroelastic contribution (note that we are under the multiplicative rule hypothesis). Afterwards, viscoelasticity explain the relaxation at medium and longer times. Table 2 collects fitting coefficients for 15 %T – 0.6% C polyacrylamide. It can be observed that viscoelastic relaxation times are higher than those obtained in 15% T – 6% C hydrogels and xerogels when they are compared at the same strain rate. This is the reason explaining different trends observed for low crosslinked hydro-gels in normalization plots in Fig. 4. Consequently, a low amount of crosslinker in the hydrogel formulation leads to an increment of the relative importance of the poroelastic behaviour. In other words, highly crosslinked polyacrylamide hydrogels are quasi - viscoelastic, while low crosslinked hydrogels have to be considered as poroviscoelastic materials at the length scale tested in this work.

Poroelastic related fitting coefficients are also included in Table 2. Interestingly, strain rate does not affect values of diffusivity and Poisson ratio. Obtained values can be contrasted to those given in the literature to provide a validation of the discrimination method presented here. T. Takigawa et al. [29] conclude that the poisson's ratio in a poly-acrylamide hydrogel similar to the highly crosslinked one used in this work is 0.457. Regarding Poisson ratio, highly crosslinked hydrogels showed higher values than those of low crosslinked materials. As the Poisson ratio at the equilibrium state is related to the compresibility change in a poroelastic material, and taking into account that at the initial load hydrogels can be considered as incompressible ($\nu_0 = 0.5$), it can be concluded that low crosslinked hydrogels exhibited a higher compressibility variation, which in turn points out the increasingly poroelastic character of these materials. The diffusivity values including in Table 2 are in agreement with those published previously in the literature [13,30]. Additionally, to check the validity range of the fitting parameters computed for hydrogels, Eq. (2) can be used to estimate the

intrinsic permeability, which in turn, depends on most of the variables collected in Table 2. Transverse elastic modulus, *G*, must be previously calculated using Eq. (15):

$$G = \frac{3P_0^{PE}}{16\,h^{3/2}R^{1/2}} \tag{15}$$

Table 2 includes G and k for high and low crosslinked hydrogels for all experimental conditions. It is clear that stiffness depends on the crosslinker agent concentration. The higher the concentration, the stiffer the hydrogel. However, the average intrinsic permeability can be calculated as $1.1 \cdot 10^{-18}$ m^2 despite of the penetration depth, or more interesting, independently on the crosslinker concentration or the strain rate. This result is in total agreement with previous literature [28,30, 31]. In Ref. [30] intrinsic permeability of polyacrylamide gels is reported as $1.4 \cdot 10^{-18}$ m^2 for a 15% of polymer whose value is pretty similar to those obtained in this work. Also, in Refs. [30,31] the intrinsic permeability was found to be independent of the amount of crosslinking which is consistent with the results obtained.

Finally, the average pore size, ξ, of hydrogels can be estimated through the permeability computed previously. Average pore size is related to intrinsic permeability through Eq. (16) referenced in Ref. [16]. Using this equation, the average pore size of the tested samples must be in the order of nm (≈ 2 nm).

$$\xi = 2\sqrt{k} \tag{16}$$

In Table 1 contact size during the relaxation test has been included for all experimental conditions. This value ranged from 110 to 141 μm for hydrogels. In any case, contact size during relaxation was several orders of magnitude higher than the pore size predicted in Eq. (16), allowing the isotropy hypothesis that was taken for the equations and methods proposed in this work.

Poisson ratio and diffusivity values of xerogels have not a physical meaning but they are simply fitting parameters showing the lack of poroelasticity for these materials.

5. Conclusions

In this work, relaxation response measured by depth sensing indentation is used to enlighten how the crosslinker concentration affects the poroviscoelastic behaviour of polyacrylamide based hydrogels. Materials with different concentration of the crosslinker agent have been synthesized. In addition, three different penetration depths have been programmed for spherical indentation relaxation tests in order to obtain not only the time dependence behaviour of hydrogels, but also the contact size influence due to poroelasticity. Several conclusions can be drawn from experimental results:

- Depth sensing indentation have been successfully used to explore intermediate length scales revealing the poroviscoelastic behaviour of Polyacrylamide hydrogels. Poroelasticity and viscoelasticy are overlapped in the global relaxation behaviour of the materials when a nanoindenter is used in the experiments.
- A load relaxation equation for a poroviscoelastic solid is used to explain the observed results. The model has been derived combining equations in the literature, with the idea that overlapping of poroelasticity and viscoelasticity can be discriminated using a multiplicative rule previously established. The relaxation equation is a highly parametrized model that can be fitted to experimental relaxation curves.
- A constrained fitting procedure has been developed to properly separate the viscoelastic and poroelastic contributions during the fitting calculations. Constrained condition is obtained by taking into account that poroelasticity is size dependent but viscoelasticity is not. Therefore, relaxation curves measured under different penetration depths are required. Methodology has been validated by
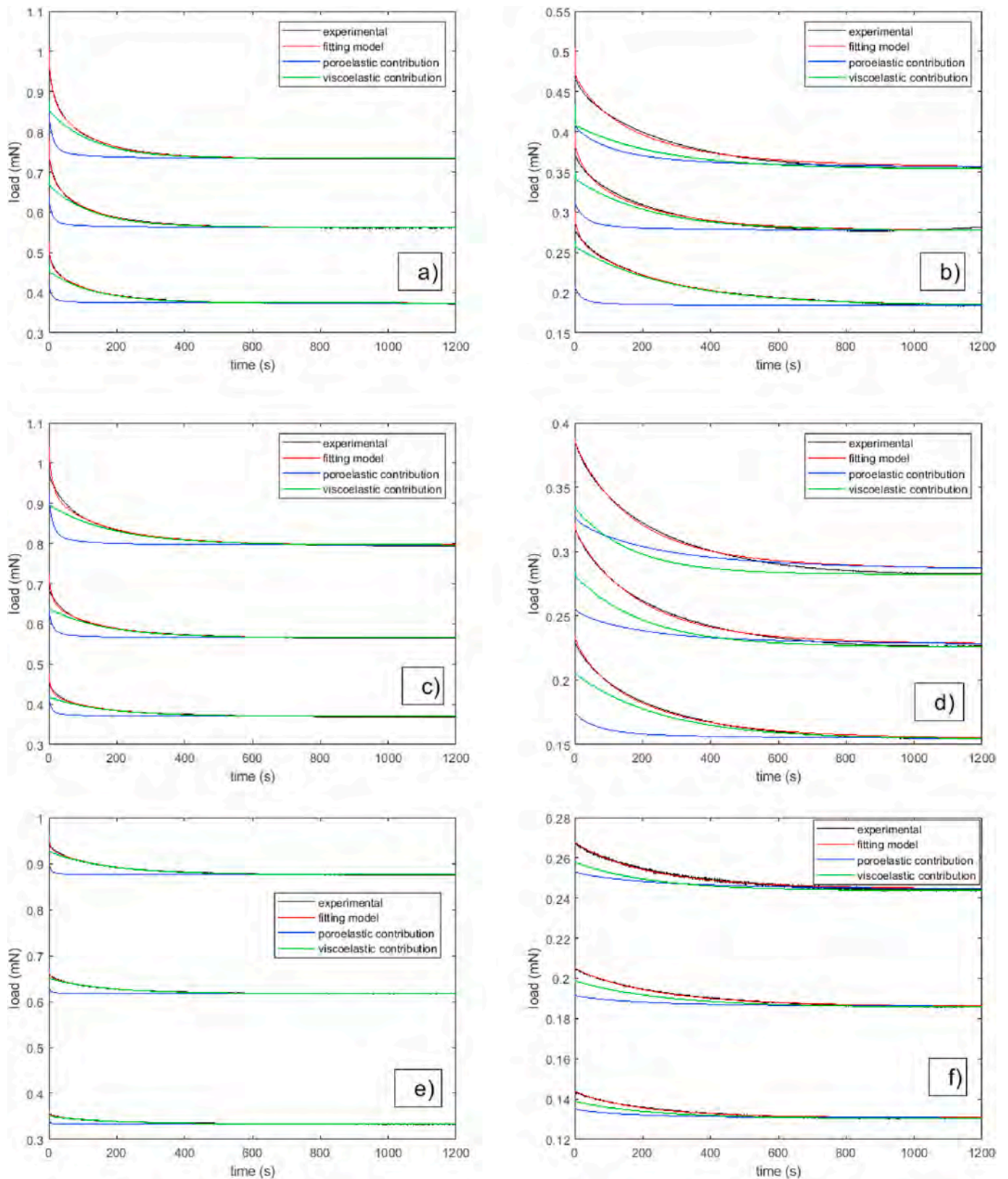
Fig. 7. Fitting model, viscoelastic and poroelastic contributions for hydrogels using constrained methodology. A) 15%T – 6%C polyacrylamide hydrogel measured at 0.17 s^{-1} of strain rate during the loading ramp. B) 15%T – 0.6%C polyacrylamide hydrogel measured at 0.17 s^{-1} of strain rate during the loading ramp c) 15%T – 6% C polyacrylamide hydrogel measured at 0.02 s^{-1} of strain rate during the loading ramp. D) 15%T – 0.6%C polyacrylamide hydrogel measured at 0.02 s^{-1} of strain rate during the loading ramp. E) 15%T – 6%C polyacrylamide hydrogel measured at 0.0027 s^{-1} of strain rate during the loading ramp. F) 15%T – 0.6%C poly-acrylamide hydrogel measured at 0.0027 s^{-1} of strain rate during the loading ramp.

Table 2

Average fitting parameters obtained for polyacrylamide based hydrogels. A 99.5% confidence interval is included in brackets for each parameter.

	strain rate of the loading ramp (s^{-1})	Fitting parameters. Average values							Derived properties	
		Penetration depth (µm)	Short relaxation time (s)	Long relaxation time (s)	Preexponential factor, A (−)	Poisson ratio at the equilibrium, ν_{inf} (−)	Diffusivity, D (µm²/s)	Initial load of the viscoelastic contribution, P_0 (mN)	Transverse Elastic Modulus, G (kPa)	Intrinsic Permeability, k (m²)
Hydrogel 15% T - 6% C	0.17	25.0	0.1	110 (97–123)	0.2831 (0.2823–0.2845)	0.4534 (0.4527–0.4544)	834 (822–849)	1.03 (1.01–1.04)	49	1.3 10⁻¹⁸
		20.0	0.1	103 (94–119)	0.3091 (0.3033–0.3099)	0.4589 (0.4567–0.4601)	812 (808–815)	0.82 (0.78–0.89)	55	1.1 10⁻¹⁸
		15.0	0.1	108 (103–110)	0.2500 (0.2486–0.2511)	0.4601 (0.4578–0.4672)	887 (880–892)	0.53 (0.49–0.61)	54	1.1 10⁻¹⁸
	0.02	25.0	0.2	112 (103–117)	0.2761 (0.2734–0.2782)	0.4632 (0.4623–0.4640)	844 (832–850)	0.98 (0.93–1.03)	47	1.1 10⁻¹⁸
		20.0	0.1	115 (111–118)	0.2803 (0.2787–0.2841)	0.4591 (0.4577–0.4599)	826 (820–830)	0.69 (0.62–0.72)	46	1.2 10⁻¹⁸
		15.0	0.1	116 (113–120)	0.3132 (0.3112–0.3141)	0.4702 (0.4691–0.4710)	877 (864–883)	0.45 (0.43–0.47)	46	1.0 10⁻¹⁸
	0.0027	25.0	0.2	131 (124–135)	0.2987 (0.2962–0.2992)	0.4675 (0.4664–0.4680)	852 (850–854)	0.93 (0.90–0.95)	44	1.1 10⁻¹⁸
		20.0	0.2	127 (122–129)	0.2786 (0.2771–0.2801)	0.4687 (0.4680–0.4697)	861 (857–865)	0.63 (0.60–0.65)	42	1.1 10⁻¹⁸
		15.0	0.2	133 (125–136)	0.2754 (0.2736–0.2766)	0.4701 (0.4695–0.4707)	867 (858–872)	0.39 (0.32–0.43)	40	1.1 10⁻¹⁸
Xerogel 15% T - 6% C	0.02	1.0	0.3	91 (87–123)	0.3533 (0.3502–0.3567)	0.4608 (0.4600–0.4612)	2765 (2713–2813)	43.12 (42.25–43.64)	–	–
		0.75	0.3	104 (95–112)	0.3066 (0.2989–0.3102)	0.4733 (0.4725–0.4740)	2812 (2765–2842)	13.39 (13.27–13.46)	–	–
		0.5	0.3	96 (89–102)	0.3387 (0.3333–0.3410)	0.4701 (0.4692–0.4709)	2656 (2599–2671)	5.10 (5.02–5.16)	–	–
	0.0027	1.0	0.2	118 (114–121)	0.3324 (0.3312–0.3356)	0.4754 (0.4745–0.4763)	3124 (3077–3209)	27.21 (27.14–27.36)	–	–
		0.75	0.3	120 (117–123)	0.3456 (0.3417–0.3470)	0.4763 (0.4750–0.4770)	3063 (2992–3098)	11.46 (11.00–11.85)	–	–
		0.5	0.2	119 (116–122)	0.3265 (0.3254–0.3273)	0.4722 (0.4716–0.4730)	3124 (3100–3143)	4.52 (4.23–4.76)	–	–
Hydrogel 15% T - 0.6% C	0.17	25.0	1.0	235 (228–238)	0.3000 (0.2929–0.3072)	0.4211 (0.4205–0.4218)	211 (198–223)	0.49 (0.47–0.50)	23	1.1 10⁻¹⁸
		20.0	1.0	234 (231–236)	0.3000 (0.2976–0.3096)	0.4189 (0.4173–0.4199)	232 (219–241)	0.35 (0.33–0.37)	23	1.2 10⁻¹⁸
		15.0	1.0	285 (267–297)	0.3000 (0.2904–0.3088)	0.4234 (0.4221–0.4240)	223 (211–227)	0.28 (0.22–0.33)	29	1.0 10⁻¹⁸
	0.02	25.0	1.0	256 (251–262)	0.2871 (0.2864–0.2888)	0.4118 (0.4108–0.4123)	221 (217–226)	0.37 (0.36–0.38)	23	1.3 10⁻¹⁸
		20.0	1.0	248 (244–252)	0.2987 (0.2972–0.2993)	0.4271 (0.4265–0.4273)	209 (202–214)	0.32 (0.30–0.35)	21	1.1 10⁻¹⁸
		15.0	1.0	261 (258–263)	0.3201 (0.3197–0.3210)	0.4255 (0.4250–0.4257)	215 (209–220)	0.24 (0.22–0.26)	25	1.0 10⁻¹⁸
	0.0027	25.0	1.0	298 (293–301)	0.3345 (0.3333–0.3351)	0.4301 (0.4292–0.4312)	234 (230–240)	0.26 (0.25–0.27)	18	1.4 10⁻¹⁸
		20.0	1.0	311 (307–314)	0.3000 (0.2990–0.3011)	0.4299 (0.4286–0.4308)	221 (216–224)	0.20 (0.18–0.21)	16	1.4 10⁻¹⁸
		15.0	1.0	301 (296–305)	0.2921 (0.2913–0.2032)	0.4323 (0.4311–0.4332)	211 (203–220)	0.14 (0.13–0.15)	18	1.2 10⁻¹⁸
Xerogel 15% T - 0.6% C	0.02	1.0	0.2	97 (88–106)	0.2683 (0.2622–0.2731)	0.4653 (0.4632–0.4667)	3112 (3086–3141)	80.76 (80.00–8103)	–	–
		0.75	0.2	127 (114–135)	0.2408 (0.2366–0.2456)	0.4711 (0.4704–0.4718)	3074 (3000–3103)	47.34 (47.11–47–54)	–	–
		0.5	0.2	103 (92–108)	0.2214 (0.2200–0.2235)	0.4723 (0.4715–0.4730)	2958 (2923–2962)	18.62 (18.43–18.69)	–	–
	0.0027	1.0	0.2	118 (116–119)	0.3022 (0.3009–0.3029)	0.4751 (0.4744–0.4757)	3028 (3002–3038)	78.68 (78.55–78.74)	–	–
		0.75	0.1	121 (118–124)	0.2928 (0.2914–0.2942)	0.4802 (0.4795–0.4810)	3051 (3036–3075)	66.53 (66.39–66.57)	–	–
		0.5	0.2	120 (116–123)	0.2789 (0.2776–0.2798)	0.4779 (0.4772–0.4784)	3142 (3100–3187)	8.72 (8.60–8.81)	–	–

applying the fitting procedure to xerogels tested in dry conditions. In these cases, the calculation drives to a curve corresponding to a pure viscoelastic solid, which is the expected result.

- Crosslinker concentration affects the mechanical behaviour of polyacrylamide hydrogels in two ways. Firstly, it is confirmed that stiffness is clearly explained through this parameter. As the

crosslinker concentration is increased hydrogels become stiffer, which is in agreement with previous literature. Secondly, viscoelasticity is the main deformation mechanism explaining the global mechanical behaviour at the intermediate length scales probed here. However, important differences can be pointed out among hydrogels with different crosslinker concentration. It should be noted that

viscoelastic relaxation times and pre-exponential factors in highly crosslinked hydrogels are very similar to those observed in xerogels. In other words, highly crosslinked polyacrylamide hydrogels can be understood as viscoelastic solids for the experimental conditions used in this work. Nevertheless, as the crosslinker concentration is reduced, the poroelastic contribution appears to be more important, doing that low crosslinked polyacrylamide hydrogels should be considered as poroviscoelastic solids. This work suggests how mechanical behaviour of polyacrylamide based hydrogels can be tailored by tuning the initial formulation of the chemical constituents.

Author's statement

C. Reinhards – Hervás: Conceptualization, Methodology, Investigation. Writing – Original Draft.

A. Rico: Conceptualization, Methodology, Formal Analysis, Writing - Review & Editing.

J. Rodríguez: Conceptualization, Methodology, Writing - Review & Editing, Funding acquisition.

Declaration of competing interest

The authors declare that they have no known competing financial interests or personal relationships that could have appeared to influence the work reported in this paper.

Acknowledgements

Appendix 1. About obtaining the Poroviscoelastic fitting equation

In a poroviscoelastic material, the viscoelastic and poroelastic contributions interact with each other to give rise to the global response. Daniel G. T. Strange et al. [12] proposes a multiplicative poroviscoelastic interaction according to Eq. A1.1.

$$P_{PVE}(t) = \frac{P_{VE}(t) \cdot P_{PE}(t)}{P_\infty^{PVE}} \tag{A1.1}$$

Where $P_{PVE}(t)$ is the poroviscoelastic load response, $P_{VE}(t)$ is the viscoelastic contribution, $P_{PE}(t)$ is the poroelastic contribution and P_∞^{PVE} is the equilibium load in the poroviscoelastic response. The use of Eq. A1.1 assumes that $P_\infty^{PVE} = P_\infty^{VE} = P_\infty^{PE} = P_\infty$.

The viscoelastic behaviour of hydrogels can be described as a Prony series [14,22–24]. In the case of using two exponential terms the viscoelastic response is expressed by Eq. A1.2.

$$P_{VE}(t) = P_\infty + \left(P_0^{VE} - P_\infty\right)\left[A\exp\left(-t/\tau_{VE1}\right) + (1-A)\exp\left(-t/\tau_{VE2}\right)\right] \tag{A1.2}$$

where P_0^{VE} is the initial load value, A is a dimensionless factor between 0 and 1, and τ_{VE1} and τ_{VE2} are the characteristic times of the viscoelastic response. Yuhang Hu et al. [19] used indentation at macroscale to characterize the poroelastic response of hydrogels. They determined that in a poroelastic material, the load relaxation is given by Eq. A1.3.

$$P_{PE}(t) = P_\infty + \left(P_0^{PE} - P_\infty\right) g(t) \tag{A1.3}$$

where P_0^{PE} is the initial load value of the poroelastic response and $g(t)$ is the poroelastic relaxation function depending of the indentation geometry.

Yuhang Hu et al. [19] determined that for a spherical indenter,

$$g(t) = 0.491 \exp\left(-0.908\sqrt{Dt/a^2}\right) + 0.509 \exp\left(-1.679\, Dt/a^2\right) \tag{A1.4}$$

where D is the difusión coefficient of the poroelastic material and a is the contact size of the indentation.

For a plane – strain cylindrical indenter,

$$g(t) = 0.791 \exp\left(-0.213\sqrt{Dt/a^2}\right) + 0.209 \exp\left(-0.95\, Dt/a^2\right) \tag{A1.5}$$

for a cylindrical punch indenter,

$$g(t) = 1.303 \exp\left(-\sqrt{Dt/a^2}\right) - 0.303 \exp\left(-0.254\, Dt/a^2\right) \tag{A1.6}$$

for a conical indenter,

$$g(t) = 0.493 \exp\left(-0.822\sqrt{Dt/a^2}\right) + 0.507 \exp\left(-1.348\, Dt/a^2\right) \tag{A1.7}$$

Also, Yuhang Hu et al. [19] determined the relation between the initial and the equilibrium loads of a poroelastic material with equilibrium Poisson ratio ν_∞ by Eq. A1.8.

$$P_0^{PE} = 2P_\infty(1 - \nu_\infty) \tag{A1.8}$$

So, introducing Eq. A1.8 in Eq. A1.3 it turns out that the poroelastic load relaxation function is

$$P_{PE}(t) = P_\infty + P_\infty(1 - 2\nu_\infty)\, g(t) \tag{A1.9}$$

Using Eq. A1.2 and Eq. A1.9 in Eq. A1.1 results;

$$P_{PVE}(t) \cdot P_\infty = P_\infty + \left(P_0^{VE} - P_\infty\right)\left[A\exp\left(-t/\tau_{VE1}\right) + (1-A)\exp\left(-t/\tau_{VE2}\right)\right] \cdot \left[P_\infty + P_\infty(1 - 2\nu_\infty)\, g(t)\right] \tag{A1.10}$$

in this way, developing the equation Eq. A1.10 equation Eq. A1.11 is obtained.

$$P_{PVE}(t) - P_\infty = \left(P_0^{VE} - P_\infty\right)\left[A\exp\left(-t/\tau_{VE1}\right) + (1-A)\exp\left(-t/\tau_{VE2}\right)\right] + P_\infty(1 - 2\nu_\infty)\, g(t)$$
$$+ \left(P_0^{VE} - P_\infty\right)\left[A\exp\left(-t/\tau_{VE1}\right) + (1-A)\exp\left(-t/\tau_{VE2}\right)\right](1 - 2\nu_\infty)\, g(t) \tag{A1.11}$$

Note that the equation Eq. A1.11 can be rewritten as,

$$P_{PVE}(t) - P_\infty = (P_{VE}(t) - P_\infty) + (P_{PE}(t) - P_\infty) + (P_{VE}(t) - P_\infty) \cdot (P_{PE}(t) - P_\infty)/P_\infty \tag{A1.12}$$

The equation Eq. A1.11 is presented as a poroviscoelastic fitting equation capable of being adjusted to obtain viscoelastic and poroelastic properties. In the case of a spherical indentation equation Eq. A1.4 must be introduced in Eq. A1.11, knowing that in this case $a^2 = Rh$, resulting in,

$$P_{PVE}(t) - P_\infty = \left(P_0^{VE} - P_\infty\right)\left[A\exp\left(-t/\tau_{VE1}\right) + (1-A)\exp\left(-t/\tau_{VE2}\right)\right] + P_\infty(1 - 2\nu_\infty)\left[0.491\exp\left(-0.908\sqrt{Dt/Rh}\right) + 0.509\exp\left(-1.679\, Dt/Rh\right)\right]$$
$$+ \left(P_0^{VE} - P_\infty\right)\left[A\exp\left(-t/\tau_{VE1}\right) + (1-A)\exp\left(-t/\tau_{VE2}\right)\right] \cdot (1 - 2\nu_\infty)\left[0.491\exp\left(-0.908\sqrt{Dt/Rh}\right) + 0.509\exp\left(-1.679\, Dt/Rh\right)\right] \tag{A1.13}$$

where R is the indenter radius and h is the penetration depth reached during the relaxation test.

Appendix 2. About obtaining the Poroviscoelastic constraint factor for indentation tests

Starting from the equation proposed by Daniel G. T. Strange et al. [12] and expressed in Appendix 1 as Eq. A1.1, the following steps are developed.

1. About the viscoelastic normalization relations.

In relaxation tests, viscoelastic behaviour can be expressed as a Prony series following the equation Eq. A2.2. This statement has been collected by numerous authors who work with hydrogels [14,23,24].

$$P_{VE}(t) = P_\infty + \left(P_0^{VE} - P_\infty\right)\sum_{i=1}^{n} A_i \exp\left(\frac{-t}{\tau_i}\right) \tag{A2.1}$$

where P_{VE}^0 is the initial viscoelastic load, A_i are a dimensionless factors that must meet that $\sum_{i=1}^{n} A_i = 1$ and τ_i are the characteristic times of the viscoelastic response.

In equation Eq. A2.1 the exponential parts are independent of the contact size, and so, for a specific material must be invariant with penetration depth, so that,

$$\frac{P_{VE}(t) - P_\infty}{P_0^{VE} - P_\infty} = \sum_{i=1}^{n} A_i \exp\left(\frac{-t}{\tau_i}\right) \tag{A2.2}$$

Using equation Eq. A1.1, the viscoelastic response can be written as,

$$P_{VE}(t) = \frac{P_{PVE}(t) \cdot P_\infty}{P_{PE}(t)} \tag{A2.3}$$

and therefore, if we multiply both sides of equality in Eq. A2.3, by a factor that normalizes the viscoelastic part, results

$$P_{VE}(t) \cdot \left(\frac{1 - P_\infty/P_{VE}(t)}{P_0^{VE} - P_\infty}\right) = \frac{P_{PVE}(t) \cdot P_\infty}{P_{PE}(t)} \cdot \left(\frac{1 - P_\infty/P_{VE}(t)}{P_0^{VE} - P_\infty}\right) \tag{A2.4}$$

so,

$$\frac{P_{VE}(t) - P_\infty}{P_0^{VE} - P_\infty} = \frac{P_{PVE}(t) \cdot P_\infty}{P_{PE}(t)} \cdot \left(\frac{1 - P_\infty / P_{VE}(t)}{P_0^{VE} - P_\infty} \right) \tag{A2.5}$$

combining equation Eq. A2.2 and equation Eq. A2.5 gives that,

$$\sum_{n=i}^{n} A_i exp\left(\frac{-t}{\tau_i}\right) = \frac{P_{PVE}(t) \cdot P_\infty}{P_{PE}(t)} \cdot \left(\frac{1 - P_\infty / P_{VE}(t)}{P_0^{VE} - P_\infty} \right) \tag{A2.6}$$

According to Eq. A1.1 it is fulfilled that $P_\infty / P_{VE}(t) = P_{PE}(t) / P_{PVE}(t)$, and so, Eq. A2.6 can be transformed to:

$$\sum_{n=i}^{n} A_i exp\left(\frac{-t}{\tau_i}\right) = \left(\frac{P_{PVE}(t) - P_{PE}(t)}{P_{PE}(t)} \right) \cdot \frac{P_\infty}{P_0^{VE} - P_\infty} \tag{A2.7}$$

M. Sakai [32] proposed Eq. A2.8 a modification of the equation developed by Sneddon in 1965 for elastic indentations valid for lineal viscoelastic materials.

$$P_{VE}(t) = C \cdot E(t) \cdot h(t)^n \tag{A2.8}$$

where C is a geometrical coefficient depending of the tip geometry, E(t) is the relaxation function, $h(t)$ is the penetration in the sample and the exponent n is a geometry coefficient depending on the tip geometry. So, in a relaxation process where a fixed penetration h is maintained Eq. A2.8 must be transformed to,

$$P_{VE}(t) = C \cdot E(t)^* \cdot h^n \tag{A2.9}$$

and so,

$$P_0^{VE} - P_\infty = C \cdot E(0)^* h^n - C \cdot E(\infty)^* \cdot h^n = C \cdot h^n \cdot (E(0)^* - E(\infty)^*) \tag{A2.10}$$

Introducing Eq. A2. 10 in Eq. A2.7 gives that

$$\sum_{n=i}^{n} A_i exp\left(\frac{-t}{\tau_i}\right) = \left(\frac{P_{PVE}(t) - P_{PE}(t)}{P_{PE}(t)} \right) \cdot \frac{P_\infty}{C \cdot h^n \cdot (E(0)^* - E(\infty)^*)} \tag{A2.11}$$

Applying Eq. A2.11 to any two penetrations (hi and hj) maintaining geometry and material the relationship Eq. A2.12 is obtained.

$$\frac{\left[\sum_{n=i}^{n} A_i exp\left(\frac{-t}{\tau_i}\right) \right]_{hi}}{\left[\sum_{n=i}^{n} A_i exp\left(\frac{-t}{\tau_i}\right) \right]_{hj}} = \frac{\left(\frac{P_{PVE}(t)_{hi} - P_{PE}(t)_{hi}}{P_{PE}(t)_{hi}} \right) \cdot \frac{P_{\infty hi}}{C_{hi} \cdot h_{hi}^{n_{hi}} \cdot (E(0) - E(\infty))_{hi}}}{\left(\frac{P_{PVE}(t)_{hj} - P_{PE}(t)_{hj}}{P_{PE}(t)_{hj}} \right) \cdot \frac{P_{\infty hj}}{C_{h=j} \cdot h_{hj}^{n_{hj}} \cdot (E(0)^* - E(\infty)^*)_{hj}}} \tag{A2.12}$$

As the viscoelastic exponential parts do not change with penetration or geometry tip, and also, $E(0)^*$ and $E(\infty)^*$ are kept constant, the Eq. A2.12 can be expressed as,

$$1 = \frac{\left(\frac{P_{PVE}(t)_{hi} - P_{PE}(t)_{hi}}{P_{PE}(t)_{hi}} \right) \cdot \frac{P_{\infty hi}}{C_{hi} \cdot h_{hi}^{n_{hi}}}}{\left(\frac{P_{PVE}(t)_{hj} - P_{PE}(t)_{hj}}{P_{PE}(t)_{hj}} \right) \cdot \frac{P_{\infty hj}}{C_{hj} \cdot h_{hj}^{n_{hj}}}} \tag{A2.13}$$

By using the equation Eq. A2.9,

$$\frac{P_{\infty hi}}{C_{hi} \cdot h_{hi}^{n_{hi}}} = \frac{P_{\infty hj}}{C_{hj} \cdot h_{hj}^{n_{hj}}} = E(\infty)^* \tag{A2.14}$$

and so, Eq. A2.13 gives that

$$\frac{P_{PVE}(t)_{hi}}{P_{PVE}(t)_{hj}} - \frac{P_{PE}(t)_{hi}}{P_{PE}(t)_{hj}} = 0 \tag{A2.15}$$

2. About the poroelastic normalization relation.

Yuhang Hu et al. [19] provided a poroelastic indentation relaxation equation expressed by Eq. A2.16, in which the function depend on the geometry and size of the indenter for a specific material and P_0^{PE} is the initial poroelastic load.

$$\frac{P_{PE}(t) - P_\infty}{P_0^{PE} - P_\infty} = g(t) \tag{A2.16}$$

In the same way as in the previous section, the expression Eq. A1.1 can be rewritten as

$$P_{PE}(t) = \frac{P_{PVE}(t) \cdot P_\infty}{P_{VE}(t)}$$ (A2.17)

Using the equation Eq. A2.17 and multiplying both sides of the equality by a factor that normalizes the poroviscoelastic loads it turns out that

$$P_{PE}(t) \cdot 2\left(\frac{1 - P_\infty/P_{PE}(t)}{P_0^{PE} - P_\infty}\right) = \frac{P_{PVE}(t) \cdot P_\infty}{P_{VE}(t)} \cdot 2\left(\frac{1 - P_\infty/P_{PE}(t)}{P_0^{PE} - P_\infty}\right)$$ (A2.18)

developing gives to,

$$2\left(\frac{P_{PE}(t) - P_\infty}{P_0^{PE} - P_\infty}\right) = \frac{P_{PVE}(t) \cdot P_\infty}{P_{VE}(t)} \cdot 2\left(\frac{1 - P_\infty/P_{PE}(t)}{P_0^{PE} - P_\infty}\right)$$ (A2.19)

so, combining Eq. A2. 16 and Eq. A2. 19 turns out that

$$2g(t) = \frac{P_{PVE}(t) \cdot P_\infty}{P_{VE}(t)} \cdot 2\left(\frac{1 - P_\infty/P_{PE}(t)}{P_0^{PE} - P_\infty}\right)$$ (A2.20)

Knowing that through the multiplicative relation Eq. A1.1 it must be fulfilled that $P_\infty/P_{PE}(t) = P_{VE}(t)/P_{PVE}(t)$ so that

$$2g(t) = \frac{P_{PVE}(t) \cdot P_\infty}{P_{VE}(t)} \cdot 2\left(\frac{1 - P_{VE}(t)/P_{PVE}(t)}{P_0^{PE} - P_\infty}\right)$$ (A2.21)

rearranging equation Eq. A2.21 is that

$$2g(t) = \frac{2P_\infty}{P_0^{PE} - P_\infty} \cdot \left(\frac{P_{PVE}(t) - P_{VE}(t)}{P_{VE}(t)}\right)$$ (A2.22)

Using the equation listed in Appendix 1 as Eq. A1.8 and developed by Yuhang Hu et al. [19] the following relationship can be found.

$$\frac{2P_\infty}{P_0^{PE} - P_\infty} = \frac{1}{\frac{P_0^{PE} - P_\infty}{2P_\infty}} = \frac{1}{\frac{P_0^{PE}}{2P_\infty} - \frac{1}{2}} = \frac{1}{1 - \nu_\infty - \frac{1}{2}} = \frac{1}{\frac{1}{2} - \nu_\infty} = \frac{2}{1 - 2\nu_\infty}$$ (A2.23)

So, recombining Eq. A2.23 in Eq. A2.21 turns out to

$$2g(t) = \frac{2}{1 - 2\nu_\infty} \cdot \left(\frac{P_{PVE}(t)}{P_{VE}(t)} - 1\right) \leftrightarrow g(t) = \frac{1}{1 - 2\nu_\infty} \cdot \left(\frac{P_{PVE}(t)}{P_{VE}(t)} - 1\right)$$ (A2.24)

rearranging equation Eq. A2.24 is that

$$P_{PVE}(t) = (1 + (1 - 2\nu_\infty) \cdot g(t)) \cdot P_{VE}(t) \leftrightarrow \frac{P_{PVE}(t)}{P_{VE}(t)} = 1 + (1 - 2\nu_\infty) \cdot g(t)$$ (A2.25)

Such that, if we divide the Eq. A2.25 corresponding to any two penetrations (h = i and h = j) each other for any geometry indentation (g1 and g2) and for the same material the relationship Eq. A2.26 is obtained.

$$\frac{P_{PVE}(t)_{hi}}{P_{PVE}(t)_{hj}} = \frac{1 + (1 - 2\nu_\infty) \cdot g1_{hi}(t)}{1 + (1 - 2\nu_\infty) \cdot g2_{hj}(t)} \frac{P_{VE}(t)_{hi}}{P_{VE}(t)_{hj}}$$ (A2.26)

So that, the relation between two poroviscoelastic relaxations must be equal to the relation of their poroelastic contribution functions as it can be seen in Eq. A2.15, so Eq. A2.26 can be rewritten as,

$$\frac{P_{PE}(t)_{hi}}{P_{PE}(t)_{hj}} = \frac{1 + (1 - 2\nu_\infty) \cdot g1_{hi}(t)}{1 + (1 - 2\nu_\infty) \cdot g2_{hj}(t)} \frac{P_{VE}(t)_{hi}}{P_{VE}(t)_{hj}}$$ (A2.27)

applying Eq. A2.16 to Eq. A2.27,

$$\frac{P_{PE}(t)_{h=i}}{P_{PE}(t)_{h=j}} = \frac{P_{\infty h=i} + (P_0^{PE}h = i - P_{\infty h=i}) \cdot g1_{h=i}(t)}{P_{\infty h=j} + (P_0^{PE}h = j - P_{\infty h=j}) \cdot g2_{h=j}(t)} = \frac{1 + (1 - 2\nu_\infty) \cdot g1_{h=i}(t)}{1 + (1 - 2\nu_\infty) \cdot g2_{h=j}(t)} \frac{P_{VE}(t)_{h=i}}{P_{VE}(t)_{h=j}}$$ (A2.28)

Knowing that by Eq. A1.8, $P_0^{PE} - P_\infty = P_\infty(1 - 2\nu_\infty)$ so Eq. A2.28 could be transformed to

$$\frac{P_{PE}(t)_{hi}}{P_{PE}(t)_{hj}} = \frac{1 + (1 - 2\nu_\infty) \cdot g1_{hi}(t)}{1 + (1 - 2\nu_\infty) \cdot g2_{hj}(t)} \cdot \frac{P_{\infty hi}}{P_{\infty hj}} = \frac{1 + (1 - 2\nu_\infty) \cdot g1_{hi}(t)}{1 + (1 - 2\nu_\infty) \cdot g2_{hj}(t)} \frac{P_{VE}(t)_{hi}}{P_{VE}(t)_{hj}}$$ (A2.29)

therefore, it must be fulfilled that,

$$\frac{P_{VE}(t)_{hi}}{P_{VE}(t)_{hj}} - \frac{P_{\infty hi}}{P_{\infty hj}} = 0 \tag{A2.30}$$

In this way, combining equations Eq. A2.15 and Eq. A2.30, a relationship is obtained that must be fulfilled for the same poroviscoelastic material when it is subjected to two different indentations (geometry or size). This equation restricts the poroviscoelastic fitting parameters valid for a good mechanical characterization.

$$\frac{P_{VE}(t)_{hi}}{P_{VE}(t)_{hj}} - \frac{P_{\infty hi}}{P_{\infty hj}} + \frac{P_{PVE}(t)_{hi}}{P_{PVE}(t)_{hj}} - \frac{P_{PE}(t)_{hi}}{P_{PE}(t)_{hj}} = 0 \tag{A2.31}$$

References

[1] S.J. Buwalda, K.W.M. Boere, P.J. Dijkstra, J. Feijen, T. Vermonden, W.E. Hennink, Hydrogels in a historical perspective: from simple networks to smart materials, J. Control. Releasae 190 (2014) 254–273.

[2] N. Chirani, L'H. Yahia, L. Gritsch, F.L. Motta, S. Chirani, S. Faré, History and applications of hydrogels, J. Biomed. Sci. 4 (2015) 2–13.

[3] F. Ullah, M.B.H. Othman, F. Javed, Z. Ahmad, H.M. Akil, Classification, processing and application of hydrogels: a review, Mater. Sci. Eng. C 57 (2015) 414–433.

[4] A.K. Denisin, B.L. Pruitt, Tuning the range of polyacrylamide gel stiffness for mechanobiology applycations, ACS Appl. Mater. Interfaces 8 (2016) 21893–21902.

[5] M. Mahinroosta, Z.J. Farsangi, A. Allahverdi, Z. Shakoori, Hydrogels as intelligent materials: a brief review of Synthesis, properties and applications, Mat, Today Chem 8 (2018) 42–55.

[6] R. Bai, Q. Yang, J. Tang, X.P. Morelle, J. Vlassak, Z. Suo, Fatigue fracture of hydrogels, EML 15 (2017) 91–96.

[7] J.-Y. Sun, X. Zhao, W.R.K. Illeperuma, O. Chaudhuri, K.H. Oh, D.J. Mooney, J. J. Vlassak, Z. Suo, Highly strechable and tough hydrogels, Nature 489 (2013) 133–136.

[8] Y. Hu, Z. Suo, Viscoelasticity and Poroelasticity in elastomeric gels, Acta Mech. Solida Sin. 25 (5) (2012) 441–458.

[9] G. Constantinides, Z.I. Kalcioglu, M. McFarland, J.F. Smith, K.J. Van Vliet, Probing mechanical properties of fully hydrated gels and biological tissues, J. Biomech. 41 (2008) 3285–3289.

[10] M.L. Oyen, Nanoindentation of hydrated materials and tissues, Curr. Opin. Solid State Mater. Sci. 19 (2015) 317–323.

[11] M.M. Fitzgerald, K. Bootsma, J.A. Berberich, J.L. Sparks, Tunable stress relaxation behaviour of an alginate – polyacrylamide hydrogel: comparison with muscle tissue, Biomacromolecules 16 (2015) 1497–1505.

[12] D.G.T. Strange, T.L. Fletcher, K. Tonsomboon, H. Brawn, X. Zhao, M.L. Oyen, Separating poroviscoelasticity deformation mechanisms in hydrogels, J. Appl. Phys. 102 (2013) 031913.

[13] D. Caccavo, S. Cascone, G. Lamberti, A.A. Barba, Hydrogels: experimental characterization and mathematical modelling of their mechanical and diffusive behavior, R. Soc. Chem 47 (2018) 2357–2373.

[14] Q.-M. Wang, A.C. Mohan, M.L. Oyen, X.-H. Zhao, Separating viscoelasticity and poroelasticity of gels with different length and times scales, AMS 30 (1) (2014) 20–27.

[15] E.P. Chan, B. Deeyaa, P.M. Johnson, Christopher M. Stafford, Poroelastic relaxation of polymer – loaded hydrogels, Soft Matter 8 (2012) 8234–8240.

[16] O. Coussy, Mechanics and Physics of Porous Solids, John Wiley & Sons, 2010.

[17] I. Argatov, G. Mishuris, Contact Mechanics of Articular Cartilage Layers: Asymptotic Models, Springer Cham, 2015.

[18] Y. Hu, X. Zhao, J.J. Vlassak, Z. Suo, Using indentation to characterize the poroelasticity of gels, Appl. Phys. Lett. 96 (2010) 121904.

[19] L. Cacopardo, N. Guazzelli, R. Nossa, G. Matte, A. Ahluwalia, Engineering hydrogel viscoelasticity, J. Mech. Behav. Biomed. Mater. 89 (2019) 162–167.

[20] M. Galli, K.S.C. Comley, T.A.V. Shean, M.L. Oyen, Viscoelastic and poroelastic mechanical characterization of hydrated gels, J. Mater. Res. Soc. 24 (3) (2009) 973–979.

[21] D. Caccavo, G. Lamberti, Poroviscoelastic model to describe hydrogels behaviour, Mater. Sci. Eng. C 76 (2017) 102–113.

[22] J.M. Mattice, A.G. Lau, M.L. Oyen, R.W. Kent, Spherical indentation load-relaxation of soft biological tissues, J. Mater. Res. Soc. 21 (8) (2006) 2003–2010.

[23] J.D. Kaufman, G.J. Miller, E.F. Morgan, C.M. Klapperich, Time-dependent mechanical characterization of poly(2-hydroxyethyl methacrylamide) hydrogels using nanoindentation and unconfined compression, J. Mater. Res. Soc. 23 (5) (2008) 1472–1481.

[24] K. Liu, T.C. Ovaert, Poro-viscoelastic constitutive modeling of unconfined creep of hydrogels using finite element analysis with integrated optimization method, J. Mech. Behav. Biomed. Mater. 4 (2011) 440–450.

[25] M.A. Biot, General theory of three – dimensional consolidation, J. Appl. Phys. 1 (2) (1941) 155–164.

[26] W. Hu, C. Corbera – Sabaté, X.D. Chen, R. Mercadé – Prieto, Poroviscoelasticity of whey protein hydrogels at different length and time scales, Food Hydrocolloids 72 (2017) 237–246.

[27] Z.I. Kalcioglu, R. Mahmoodian, Y. Hu, Z. Suo, K.J. Van Vliet, From macro- to microscale poroelastic characterization of polymeric hydrogels via indentation, Soft Matter 8 (2012) 3393–3398.

[28] T. Toshikazu, Y. Morino, K. Urayama, T. Masuda, Poisson's ratio of Polyacrylamide (PAAm) gels, Polym. Gels Netw. 4 (1996) 1–5.

[29] M.L. White, The permeability of an acrylamide polymer gel, J. Phys. Chem. 64 (10) (1960) 1563–1565.

[30] M.L. Oyen, Mechanical characterisation of hydrogel materials, Int. Mater. Rev. 59 (1) (2014) 44–59.

[31] M. Sakai, Time-dependent viscoelastic relation between load and penetration for an axisymmetric indenter, Philos. Mag. A 82 (10) (2002) 1841–1849.